

# Radiomics-based quantitative contrast-enhanced CT analysis of abdominal lymphadenopathy to differentiate tuberculosis from lymphoma

Meng-Ting Shen,<sup>1</sup> Xi Liu,<sup>1,2</sup> Yue Gao,<sup>1</sup> Rui Shi,<sup>1</sup> Li Jiang,<sup>1</sup> Jin Yao<sup>1,\*</sup>

<sup>1</sup>Department of Radiology, West China Hospital, Sichuan University, Chengdu 610041, China

<sup>2</sup>Key Laboratory of Carcinogenesis and Translational Research (Ministry of Education), Department of Radiology, Peking University Cancer Hospital and Institute, Beijing 100142, China

\*Corresponding author. Jin Yao, [shelleyyao@163.com](mailto:shelleyyao@163.com)

Dear Editor,

Tuberculosis (TB) is a significant cause of morbidity and mortality in developing countries, with a global burden of ~10.0 million cases in 2019. China accounts for 8.4% of TB cases globally, ranking third after India and Indonesia [1]. Abdominal TB is a common extrapulmonary manifestation, often presenting as lymphadenopathy. Accurate differentiation between abdominal tuberculosis lymphadenopathy (ATBL) and lymphoma holds significance for treatment decisions and prognosis. Numerous case reports highlight the challenge of misdiagnosing TB as lymphoma due to the overlapping imaging characteristics of these diseases, presenting a hurdle for conventional computed tomography (CT) methods [2–4]. Radiomics, an automated extraction of imaging features, offers a promising solution. While prior radiomics studies focused on lymphoma and lymph node (LN) metastasis, the application of radiomics to differentiate ATBL and lymphoma in abdominal sites has not been explored [5, 6]. Here, we retrospectively included 107 patients with confirmed ATBL and 194 patients with lymphoma affecting the abdominal LNs. We proceed to develop and validate a radiomics-based model, using contrast-enhanced CT (CECT) images, to accurately differentiate between abdominal lymphadenopathy associated with TB and lymphoma.

The diagnosis criteria for ATBL included histopathologically confirmed caseating granulomas and bacteriological identification of mycobacterium tuberculosis [7]. Lymphoma was histopathologically confirmed by means of biopsy of enlarged LNs. The criteria were as follows: (i) other neoplastic diseases, opportunistic infections, liver cirrhosis, or hepatitis; (ii) LNs with calcification; (iii) LNs minimum diameter not >1.0 cm; and (iv) poor image quality. Radiological CT features were analysed by two radiologists, including LN distribution, diameter, and enhancement patterns. The LN distribution included areas such as the hepatoduodenal ligament, the hepatogastric ligament, the gastrosplenic ligament, the anterior pararenal space, the upper and lower para-aortic regions, the mesentery, and the greater omentum [8]. Blinded to clinical data, two radiologists performed 3D segmentation of the volumes of interest (VOIs) using 3D Slicer software

(Fig. 1). All images were resampled to a  $1 \times 1 \times 1$  mm voxel size to partially counter the heterogeneous reconstruction settings. The voxel values were aggregated into bins 25 Hounsfield Unit (HU) wide to reduce the interference of image noise and normalize intensities. The logistic regression (LR) and the support vector machine (SVM) were applied for selecting predictive radiomics signature. Clinical (selected clinical and radiological features), radiomic (selected radiomic features), and combined (selected clinical, radiological, and radiomic features) predictive models were developed. All statistical analyses, feature selection, and modelling were performed in R (version 4.0.3, <http://www.r-project.org>). A two-tailed  $P$  value < 0.05 was considered significant.

All subjects were randomly divided into a training set ( $n = 209$ ) and a validation set ( $n = 92$ ) (supplementary Table 1, see online supplementary material). A total of 1130 radiomics features were initially extracted, categorized into shape-based features, first-order statistics, texture features [e.g. gray-level co-occurrence matrix (GLCM), gray-level dependence matrix (GLDM), gray-level run-length matrix (GLRLM), gray-level size zone matrix (GLSZM), neighborhood gray-tone difference matrix (NGTDM)], and transformed features. After the removal of 222 features due to poor reproducibility, 908 features proceeded to multistep dimension reduction. At the end of the process, the 8 most important and independent features were selected, including 1 shape feature (major axis length), 3 first-order features (kurtosis, skewness, 90 percentile), and 4 texture features (dependence non-uniformity normalized, small area emphasis, run entropy, Imc2) (supplementary Table 2, see online supplementary material). The Radscores showed significant differences between ATBL and lymphoma in both training ( $0.0752 \pm 0.8898$  vs  $-1.0891 \pm 0.7184$ ,  $P < 0.001$ ) and validation ( $0.1754 \pm 0.7628$  vs  $-1.1495 \pm 0.5783$ ,  $P < 0.001$ ) sets.

The radiomic signature, evaluated by LR analyses, demonstrated favorable discriminatory ability with areas under curves (AUCs) of 0.91 and 0.86 in the training and validation sets, respectively. Accuracy, sensitivity, and specificity were notable at 88%, 76%, and 94% in the training set and 83%, 72%, and 88% in the validation set. The performance of the SVM algorithm was

Received 26 December 2023; accepted 22 January 2024. published 1 February 2024

© The Author(s) 2024. Published by Oxford University Press on behalf of the West China School of Medicine & West China Hospital of Sichuan University. This is an Open Access article distributed under the terms of the Creative Commons Attribution-NonCommercial License

(<https://creativecommons.org/licenses/by-nc/4.0/>), which permits non-commercial re-use, distribution, and reproduction in any medium, provided the original work is properly cited. For commercial re-use, please contact [journals.permissions@oup.com](mailto:journals.permissions@oup.com)

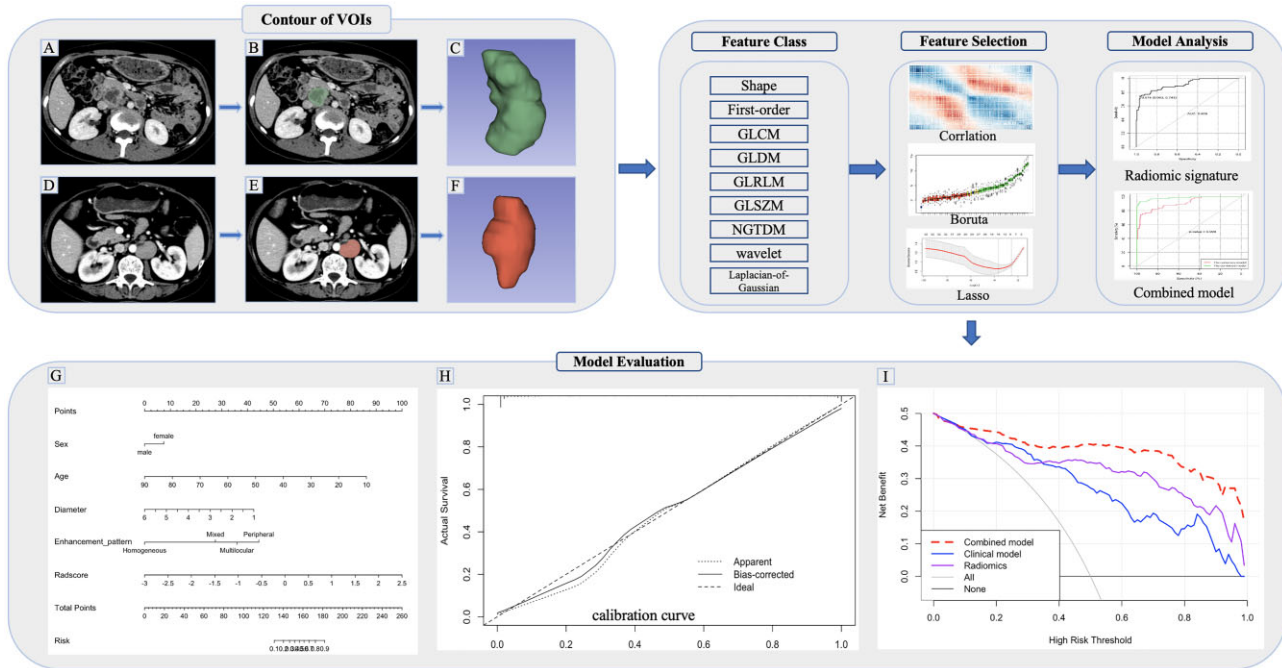


**Figure 1.** Radiomics workflow. (A) Venous-phase CECT image in a 15-year-old male with ATBL. (D) Venous-phase CECT image in a 55-year-old woman with lymphoma. (B, E) Axial venous-phase CECT image marked with a VOI. (C, F) 3D model of VOI. (G) Nomogram for differentiation between ATBL and lymphoma was established using the training cohort, with Radscore, sex, age, LN diameter, and LN enhancement pattern. (H) Calibration curves of the radiomics nomogram in the training. (I) Decision curve analysis of the models. The y-axis indicates net benefit to patients. Across the threshold probability, the application of a nomogram to differentiate lymphoma from ATBL provides more benefit than clinical and radiomics alone.

similar to that of the LR analysis, with an AUC of 0.91 in the training set and 0.87 in the validation set. Univariable analysis identified age, sex, LN diameter, and enhancement patterns as significant between ATBL and lymphoma ( $P < 0.05$ ). The clinical model with these characteristics performed equally well compared to the radiomic model in distinguishing ATBL from lymphoma in the training and validation cohorts (supplementary Table 3, see online supplementary material).

Notably, the AUCs for the combined model were 0.96 in the training set and 0.92 in the validation set, with sensitivity, specificity, and accuracy at 85%, 95%, and 91% in the training set, and 76%, 86%, and 83% in the validation set. In both sets, AUC values for the combined model significantly surpassed those of the radiomic and clinical model ( $P < 0.05$ ). The combined model was developed and presented as the nomogram, and the calibration curve of the nomogram demonstrated great agreement in the training cohort. Decision curve analysis indicated the nomogram's superior net benefit across threshold probabilities in distinguishing ATBL from lymphoma compared to other methods (Fig. 1).

This study underscores the effectiveness of machine learning-assisted radiomic-based quantitative CECT analysis in accurately distinguishing between ATBL and lymphoma. Run entropy measures the uncertainty/randomness in the distribution of run lengths and gray levels. Dependence non-uniformity normalized measures the similarity of dependence throughout the image. Our study showed higher run entropy in ATBL patients and higher dependence non-uniformity normalized in lymphoma patients, suggesting greater heterogeneity in texture patterns and increased homogeneity among dependencies in ATBL, possibly linked to the complex pathophysiological process of TB. The TB lymphadenopathy's different pathological stages [9], character-

ized by varying enhancement patterns, provide additional insights into disease progression.

Another feature that has to be mentioned is shape. The feature of major axis length yields the largest axis length of the region of interest (ROI)-enclosing ellipsoid and is calculated using the largest principal component. In the present study, ATBL patients had lower major axis lengths than lymphoma patients. This may be because TB is a pathologically self-limiting growth disease. This aligns with the self-limiting growth nature of TB, where enlarged LN diameters are consistently  $< 4$  cm (average 1.5 cm), contrasting with the rapid growth and larger nodes observed in lymphoma [9].

A radiomic model combined with machine learning is non-invasive and can be performed on images obtained in clinical work. This study observed fairly consistent performance using two different classic machine learning approaches (LR and the SVM algorithm), which increases confidence in the results obtained. A nomogram integrating radiomic signature, LN diameter, LN enhancement pattern, sex, and age yields excellent differentiation ability, with an AUC of 0.92 in the validation cohort. The combined model surpasses the individual radiomic and clinical models in differential diagnosis, serving as a valuable non-invasive tool for accurate differentiation between ATBL and lymphoma when clinical information and CT images are available. Finally, due to the retrospective single-center nature of our study design, these findings require external validation to assess their reproducibility and clinical applicability.

In conclusion, we first explored the performance of CECT radiomic features in differentiating TB from lymphoma involving abdominal LNs. The combined model, incorporating radiomic features and clinical characteristics, emerges as a powerful tool for precise and convenient differential diagnosis, offering valuable insights for precision medicine.

## Acknowledgments

This work was supported by the Sichuan Province Science and Technology Support Program (Grant No. 2020YFS0120).

## Author contributions

MS and JY conceived and designed the study and prepared the manuscript. XL provided substantive editing. YG, RS and LJ performed the manuscript review and data analysis. JY assisted in conducting the manuscript revision. All authors read and approved the final manuscript.

## Supplementary data

Supplementary data is available at [PCMED](#) online.

## Conflict of interest statement

All authors declare no conflicts of interest in relation to this work.

## References

1. *Global tuberculosis report 2020*. Geneva: World Health Organization; 2020. Licence: CC BY-NC-SA 3.0 IGO. Available via <https://www.who.int/teams/global-tuberculosis-programme/data>.
2. Gong Y, Li S, Rong R et al. Isolated gastric varices secondary to abdominal tuberculosis mimicking lymphoma: a case report. *BMC Gastroenterol* 2019;**19**:78. <https://doi.org/10.1186/s12876-019-0998-9>
3. Akdogan RA, Halil Rakici AA, Güngör S et al. F-18 fluorodeoxyglucose positron emission tomography/computed tomography findings of isolated gastric tuberculosis mimicking gastric cancer and lymphoma. *Euroasian J Hepatogastroenterol* 2018;**8**:93–6. <https://doi.org/10.5005/jp-journals-10018-1270>
4. Collu C, Fois A, Crivelli P et al. A case-report of a pulmonary tuberculosis with lymphadenopathy mimicking a lymphoma. *Int J Infect Dis* 2018;**70**:38–41. <https://doi.org/10.3389/fpubh.2016.00031>
5. Bayanati H, E Thornhill R, Souza CA et al. Quantitative CT texture and shape analysis: can it differentiate benign and malignant mediastinal lymph nodes in patients with primary lung cancer? *Eur Radiol* 2015;**25**:480–7. <https://doi.org/10.1007/s00330-014-3420-6>
6. Forghani R, Chatterjee A, Reinhold C et al. Head and neck squamous cell carcinoma: prediction of cervical lymph node metastasis by dual-energy CT texture analysis with machine learning. *Eur Radiol* 2019;**29**:6172–81. <https://doi.org/10.1007/s00330-019-06159-y>
7. Lal SB, Bolia R, Menon JV et al. Abdominal tuberculosis in children: A real-world experience of 218 cases from an endemic region. *JGH Open* 2020;**4**:215–20. <https://doi.org/10.1002/jgh3.12245>
8. Li Y, Yang ZG, Guo YK et al. Distribution and characteristics of hematogenous disseminated tuberculosis within the abdomen on contrast-enhanced CT. *Abdom Imaging* 2007;**32**:484–8. <https://doi.org/10.1007/s00261-006-9144-6>
9. De Backer AI, Mortelé KJ, Deeren D et al. Abdominal tuberculous lymphadenopathy: MRI features. *Eur Radiol* 2005;**15**:2104–9. <https://doi.org/10.1007/s00330-005-2745-6>